



Journal of Applied and Computational Mechanics



Research Paper

On the Problem of Modeling High Strain-Rate Behavior of Ice

Andrey Yu Kuchmin¹, Andrey K. Abramyan²

Institute for Problems in Mechanical Engineering of the Russian Academy of Science (IPMash RAS), Bolshoy prospekt V.O., 61, Saint-Petersburg, 199178, Russia,
E-mail: radiotelescope@yandex.ru (A.Yu.K.); andabr55@gmail.com (A.K.A.)

Received April 11 2024; Revised June 05 2024; Accepted for publication June 23 2024.
Corresponding author: A.K. Abramyan (andabr55@gmail.com)
© 2024 Published by Shahid Chamran University of Ahvaz

Abstract. A model of freshwater ice behavior under impact compression is suggested. To obtain the parameters (mechanical properties of ice at high-speed loading) of the model the Kolsky method is used. The necessary parameter data are obtained at a strain rate of $1.4 \times 10^3 \text{ s}^{-1}$. A new procedural approach and an experimental data filtering algorithm are proposed. In addition, a phenomenological model of ice is offered, which makes it possible to obtain a relationship between the measured force and the parameters of the material. The verification of the model is performed according to the results of experiments in which forces are obtained in the study of the destruction of ice samples for high strain rates. It is shown that the analytical force model describes the experimental data well.

Keywords: Ice; high strain-rate behavior; uniaxial compression; Hopkinson–Kolsky bar; ice fracture.

1. Introduction

Over the past 60 years, a considerable amount of research has been conducted on the mechanical properties of ice, mainly freshwater ice. Although ice is a well-known material, its properties are not fully understood. An analysis of known publications on the dynamic strength of ice shows that there is a large variation in the measured parameters, since the quantitative values are influenced by the test procedure [1]. In addition, temporal processes play a significant role.

Reviews of previous work on this topic were presented in [1-5]. One of the problems in studying the process of ice destruction is the determination of its dynamic strength at a high strain rate. In the process of developing a constitutive model for ice behavior under dynamic loading, the main problems that arise are how to consider micromechanisms of plastic deformation. Since different mechanisms of dynamic deformation usually operate simultaneously and can vary depending on the strain rate, it does not seem possible to use only a deterministic approach. The decisive influence of the ice microstructure on ice destruction, as well as the temporary strength and the stress transfer process, was shown in [6]. For polycrystalline ice, it seems impossible to obtain the relationship between the dynamic characteristics at the macroscopic scale and the microlevel using the continuum theory of dislocations. We discuss the latest experimental and theoretical results concerning the mechanical properties of ice under dynamic loading and their applications. First, we mention the problem of ice crystal icing in aircrafts occurring in the clouds at cruise altitudes [7-10]. A model describing ice accretion in turbofan engines was developed to predict ice thickness and shape [11]. To model the velocity components of ice crystals colliding with the surface of a blunt-nosed body, a model describing two-phase flow was proposed [12]. Ice crystals with diameters between 5 μm and 2 mm and impact velocities between 50 and 250 m/s adhere to the surfaces on which they impinge [13, 14]. This problem stimulates the study of the impact of ice particles on a solid surface [15-17]. On Enceladus, the moon of Saturn, ice particle plumes emerge from the south polar region, and to realize a space mission to Saturn, it is necessary to study the impact of ice particles on the spacecraft, which was performed in previous works [17, 18]. It was shown that pure water ice grains with a diameter of $\sim 700 \text{ nm}$ experience rebound, adhesion, and fragmentation at impact velocities below 400 m/s, between 400 and 800 m/s, and above 800 m/s, respectively, when colliding with a metallic target at a velocity of 0.2-2.4 km/s. A constitutive model was developed to study the failure mechanisms of space structural materials under the hypervelocity impact of ice [19]; it was shown that the damage results from the competition between fracture, plasticity, and phase transition in the materials.

Possible damage by hail was discussed in [20] by analyzing the peak force and time of occurrence generated by ice balls with diameters ranging from 31.8 to 50.8 mm colliding with a rigid target. The authors described the empirical relationships between the peak force and the impact velocity, ice ball radius, ice density, and mechanical properties of ice. Roisman developed a hydrodynamic model that describes the deformation and subsequent fragmentation of a spherical ice particle as a result of a collision with a perfectly rigid substrate [21]. Ice particle fragmentation resulting from impact on a solid wall was studied using a semi-empirical model to predict the size of the largest reemitted fragment [22]. A solid residual ice cone that remains attached to the substrate after ice particle impact was studied in [23].

During mining in cold regions, frozen, water-saturated soil is subjected to dynamic loads due to drilling and blasting. In these applications, the multiaxial and cyclic impact loading of frozen soil containing ice crystals has been studied [24-27].



The split Hopkinson pressure bar (SHPB) system is widely used to study the mechanical response of ice under compressive dynamic loading [28-33]. Other deformation modes such as tension [34-36] and bending [37] are also analyzed. Energy dissipation through the ice-cotton composite was studied as a function of freezing temperature and cotton content [38].

SHPBs were used to study the dynamic strength of differently prepared ice under uniaxial compression at temperatures ranging from 173-263 K and at strain rates up to 10^3 s^{-1} [39]. It was shown that the peak compressive strength of ice is a linear function of density; the pure high density (porous low density) ice showed a peak compressive strength of $49.5 \pm 2.0 \text{ MPa}$ ($36.5 \pm 1.9 \text{ MPa}$); no effect of the strain rate was observed [39].

To validate the model proposed in the paper, the results of the high strain rate uniaxial compression test are used. The Kolsky method was used in our research with the help of the SHPB. The compression tests are performed in the traditional way as in [40-46]. The novelty with respect to the abovementioned works is that we propose a new method of test data analysis. This new method helps, in our opinion, to obtain a better analysis of the information received in tests about the deformation process.

Finally, a phenomenological model of ice is proposed. In our work we include micromechanics in the description of the process of dynamic deformation. In this context, one of the experimental problems is the propagation of a steady elastoplastic wave. The verification of the model is carried out according to the results of experiments, during which the forces acting on ice samples are measured. This approach allows us to obtain a relationship between the measured force and the parameters of the material, taking into account the loading modes.

2. Experimental Methods

To test ice samples at high strain rates we used the Kolsky method. The tests are performed under compression in the traditional way. As a result of the tests, dependences are obtained in the form of graphs necessary to assess the strength of materials under the action of dynamic loads.

A schematic diagram of the split Hopkinson pressure bar apparatus is shown in Fig. 1, where: 1 – gas gun with a pressure control system, 2 – striker, 3 – incident bar, 4 – strain gauges, 5 – transmitted bar, 6 – specimen, 7 – trigger, 8 – computer with data acquisition system, 9 – calibration and information collection circuit, 10 – clock pulse generator.

For uniaxial compression tests, the classical Kolsky scheme is used. The sample is located between the bars. The bars are used to transmit a stress pulse to the sample, as well as to record the parameters of this pulse. The collision of the striker with the incident bar leads to the formation and propagation of a compression wave in this bar. Part of the wave passes into the sample, and the other part is reflected at the boundary of the sample and the bar. Strain pulses in the incident and transmitted bars were measured using foil strain gauges (or semiconductor strain gauges) glued to the outer surface of the rods. To compensate for bending vibrations in the rods and increase the amplitude of the useful signal in the working sections, 4 strain gauges connected in series are glued. A strain gauge in the incident bar rod is used to record the loading and reflected pulses; the transmitted pulse is recorded on the transmitted bar. Electrical signals from strain gauges are received and processed by a computer through a calibration and information acquisition circuit, taking into account their reference to a time scale based on synchronizing pulses from the generator. Receiving and recording equipment introduces errors and distortions that significantly affect the accuracy of determining characteristics.

Distilled water was used to remove 20 ice samples. The freezing of water was carried out in a freezer of temperature 20°C . The density of ice samples is determined, and several ice samples of known geometry are made (cylinders with a diameter of 20 mm and length of 45 mm). The density of the ice samples was 0,90 at 0,92 g/cm^3 . The sample fabrication methods used were as follows. For testing, sets of thin-walled metal clips of the required configuration are made. These clips are fixed on a flat plate with glue. Distilled water is poured into the clips up to the upper cut of the clips, and the plate is placed in a freezer for 2 days. During the process of water freezing, the volume of the sample increases and the protruding part of the ice sample is removed. Next, the samples are removed from the holders and placed in a polyurethane foam container for storage, which remains in the freezer all the time. To avoid the appearance of cracks in the samples, the rate of water freezing was reduced by using a heat-insulating polyurethane foam cap, placed on a set of clips with water. For the compression tests, tablets ~20 mm high and ~40 mm in diameter were used. The length of the high-strength aluminum alloy striker bar is 0.3 m, and the lengths of the incident and transmitter bars are 1.6 m and 1.8 m, respectively.

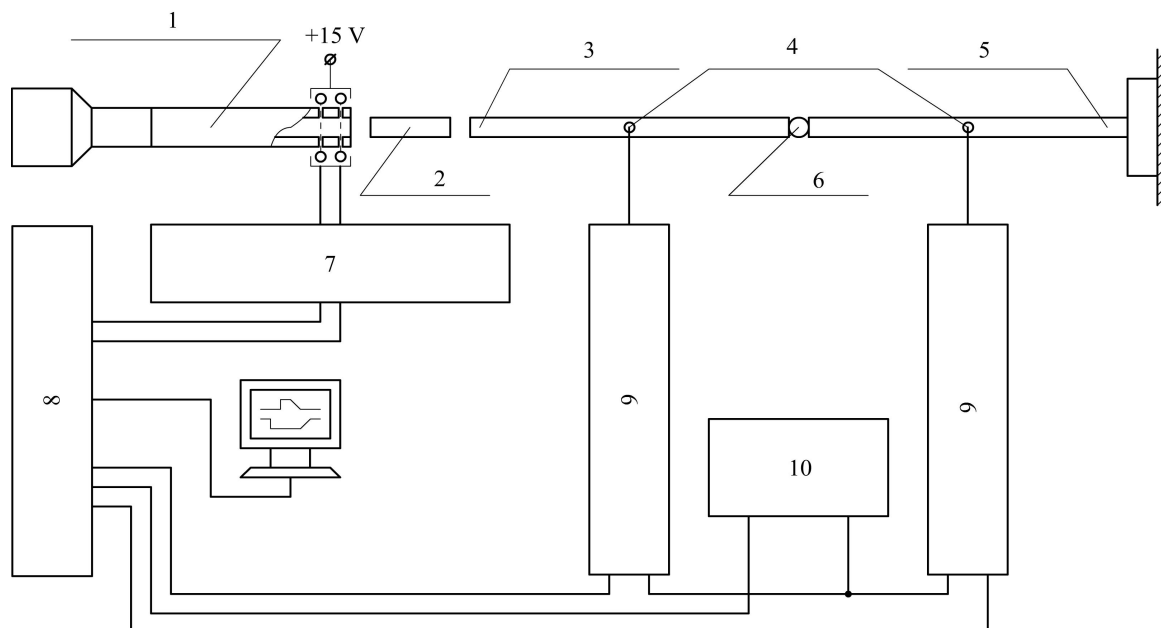


Fig. 1. Split Hopkinson pressure bar facility.



Liquid nitrogen is used to prevent sample heating during test preparation and to cool the edges of the measuring rods. A special chamber is made, lined inside with a layer of polyurethane foam to reduce the penetration of heat from the environment. The edges of the measuring rods were placed in the chamber. The chamber was purged with liquid nitrogen vapor which helped maintain the required negative temperature. The sample temperature is measured using a type E thermocouple, the signal from which is transmitted to a digital millivoltmeter. The thermocouple is located inside the chamber directly in the zone of contact of one of the measuring rods with the sample. To record the pulse transmitted through the sample glued semiconductor gauges are used.

3. Method of Analysis of Experimental Data

All tests were performed at strain rate of $\sim 1.4 \cdot 10^3 \text{ s}^{-1}$ under compression. An example of a typical graph obtained using traditional methods for processing data from experiments carried out according to the Hopkinson scheme is shown in Fig. 2. This figure shows the dependence of the stresses on time for ice at a temperature of -15°C and a strain rate of $1.4 \cdot 10^3 \text{ s}^{-1}$. These dependencies are obtained after processing the signals from the strain gauges.

To determine the value of the stress at the moment of destruction, it is necessary to know the maximum value of the stress during dynamic compression and the time when this maximum value is reached. As shown in Fig. 1, several maxima are observed on the graph. This raises the question of the nature of the occurrence of these maxima. The solution to this question will allow the selection of one of the maxima corresponding to the moment of destruction of the material. The experimental data filtering algorithm proposed in this article makes it possible to justify the choice of the stress maximum.

3.1. Single pulse filtering and analysis

Various methods for the end-to-end calibration of Hopkinson's experimental setups are known [40-44]. These methods, however, do not eliminate a number of factors: such as the spread of loading pulse shapes, inaccuracies in the timing of pulses and the presence of noise components, to which methods for calculating the strength characteristics of materials are sensitive. Therefore, it is necessary to use digital signal processing methods for filtering and analyzing experimental data as an interconnected triad of loading, reflected, and transmitted pulses. The analysis of the experimental data y as a function of time t for the loading and transmitted pulses makes it possible to distinguish three characteristic regions for the filtered pulse (see Fig. 3):

- 1) the derivative of the momentum increases monotonically;
- 2) the derivative of the momentum decreases monotonically;
- 3) the derivative of the momentum increases monotonically.

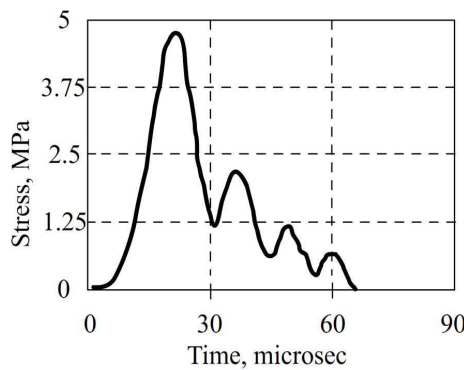


Fig. 2. Stress as a function of time under dynamic compression at the strain rate of $1.4 \cdot 10^3 \text{ s}^{-1}$.

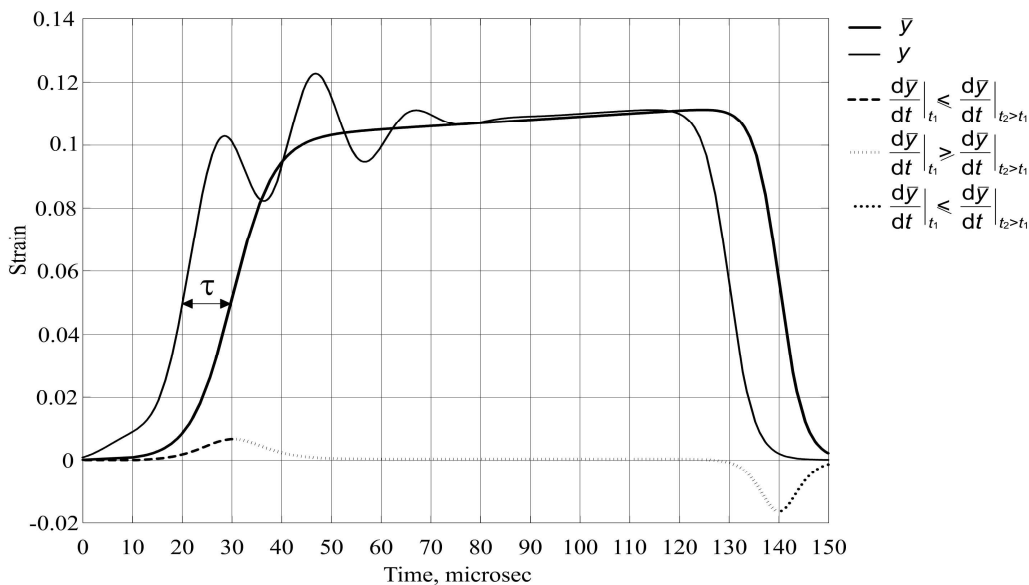


Fig. 3. Analyzed impulses and their derivatives.



This property of the signal can be used as a criterion for filtering, in particular, to determine the floating average \bar{y} . In mathematical form, the criterion for dividing into oscillations and floating average can be written as follows:

$$J = \min_{\bar{y}} \left\{ \int_{t_0}^{t_k} (y - \bar{y})^2 dt + \int_{t_0}^{t_k} \left(\frac{dy}{dt} - \frac{d\bar{y}}{dt} \right)^2 dt \right\}, \tag{1}$$

with restrictions,

$$\begin{aligned} \frac{d^2}{dt^2} \bar{y} \geq 0, t \in \left[t_0, t_{\max(\frac{d\bar{y}}{dt})} \right], \frac{d^2}{dt^2} \bar{y} \leq 0, \\ t \in \left[t_{\max(\frac{d\bar{y}}{dt})}, t_{\min(\frac{d\bar{y}}{dt})} \right], \frac{d^2}{dt^2} \bar{y} \geq 0, t \in \left[t_{\min(\frac{d\bar{y}}{dt})}, t_k \right]. \end{aligned} \tag{2}$$

With numerical implementation expressions (1) and (2) can be reduced to a quadratic programming problem. Let us move from a continuous representation of the functions (1) and (2) to a discrete representation. For this we represent t , y and \bar{y} as lattice functions in the form of a sequence of readings t , y and \bar{y} .

Then, Eq. (1) will take the form:

$$J = \min_{\bar{y}} \left\{ (\mathbf{y} - \bar{\mathbf{y}})^T (\mathbf{y} - \bar{\mathbf{y}}) + (\Delta \mathbf{y} - \Delta \bar{\mathbf{y}})^T (\Delta \mathbf{y} - \Delta \bar{\mathbf{y}}) \right\}, \tag{3}$$

where Δy and $\Delta \bar{y}$ are the finite differences of the corresponding quantities. Using the properties of finite differences (4):

$$\begin{aligned} \Delta y[k] = y[k] - y[k-1], \Delta \bar{y}[k] = \bar{y}[k] - \bar{y}[k-1], \Delta \mathbf{y} = \mathbf{H}_1 \mathbf{y}, \Delta \bar{\mathbf{y}} = \mathbf{H}_1 \bar{\mathbf{y}}, \\ \mathbf{H}_1 = \begin{bmatrix} -1 & 1 & 0 & 0 & 0 \\ 0 & -1 & 1 & 0 & 0 \\ 0 & 0 & -1 & 1 & 0 \\ & & & \ddots & \\ 0 & 0 & 0 & -1 & 1 \end{bmatrix}_{(n-1) \times n}, \end{aligned} \tag{4}$$

and then after simplification of Eq. (3) one can obtain:

$$\begin{aligned} J = \min_{\bar{y}} \left\{ (\mathbf{y} - \bar{\mathbf{y}})^T (\mathbf{y} - \bar{\mathbf{y}}) + (\Delta \mathbf{y} - \Delta \bar{\mathbf{y}})^T (\Delta \mathbf{y} - \Delta \bar{\mathbf{y}}) \right\} = \\ = \min_{\bar{y}} \left\{ (\mathbf{y} - \bar{\mathbf{y}})^T [\mathbf{I} + \mathbf{H}_1^T \mathbf{H}_1] (\mathbf{y} - \bar{\mathbf{y}}) \right\} = \min_{\mathbf{x}} \left\{ \mathbf{x}^T [\mathbf{I} + \mathbf{H}_1^T \mathbf{H}_1] \mathbf{x} \right\}, \end{aligned} \tag{5}$$

where $\mathbf{x} = \mathbf{y} - \bar{\mathbf{y}}$ is a new variable, n is the sample size, and \mathbf{I} is the identity matrix of dimension $n \times n$. Using Eqs. (4) and (5), we rewrite constraint (2) in the following form:

$$\begin{aligned} \Delta^2 \bar{y}[k] \geq 0, k \in [3, k_{\max(\Delta \bar{y})}], \Delta^2 \bar{y}[k] \leq 0, k \in [k_{\max(\Delta \bar{y})}, k_{\min(\Delta \bar{y})}], \\ \Delta^2 \bar{y}[k] \geq 0, k \in [k_{\min(\Delta \bar{y})}, k_k]. \end{aligned} \tag{6}$$

Using the properties of the second finite differences (7) one obtains:

$$\begin{aligned} \Delta^2 y[k] = \Delta y[k] - \Delta y[k-1] = y[k] - 2y[k-1] + y[k-2], \\ \Delta^2 \mathbf{y} = \mathbf{H}_2 \mathbf{y}, \Delta^2 \bar{\mathbf{y}} = \mathbf{H}_2 \bar{\mathbf{y}}, \\ \mathbf{H}_2 = \begin{bmatrix} 1 & -2 & 1 & 0 & 0 & 0 \\ 0 & 1 & -2 & 1 & 0 & 0 \\ 0 & 0 & 1 & -2 & 1 & 0 \\ & & & \ddots & & \\ 0 & 0 & 0 & 1 & -2 & 1 \end{bmatrix}_{(n-2) \times n}, \end{aligned} \tag{7}$$

and after the simplification of expression (6) we have:

$$\begin{aligned} \gamma \mathbf{H}_2 \bar{\mathbf{y}} \leq 0, \\ \gamma = \begin{bmatrix} -\mathbf{I}_{(n_{\max(\Delta \bar{y})}-2) \times (n_{\max(\Delta \bar{y})}-2)} & 0 & 0 \\ 0 & \mathbf{I}_{(n_{\min(\Delta \bar{y})}-n_{\max(\Delta \bar{y})}) \times (n_{\min(\Delta \bar{y})}-n_{\max(\Delta \bar{y})})} & 0 \\ 0 & 0 & -\mathbf{I}_{(n-n_{\min(\Delta \bar{y})}) \times (n-n_{\min(\Delta \bar{y})})} \end{bmatrix}. \end{aligned} \tag{8}$$

Using the substitution $\mathbf{x} = \mathbf{y} - \bar{\mathbf{y}}$, we reformulate Eqs. (1) and (2) as a quadratic programming problem with respect to \mathbf{x} :

$$J = \min_{\mathbf{x}} \left\{ \mathbf{x}^T [\mathbf{I} + \mathbf{H}_1^T \mathbf{H}_1] \mathbf{x} \right\}, \tag{9}$$

with constraints:



$$\gamma \mathbf{H}_2 \mathbf{x} \geq \gamma \mathbf{H}_2 \mathbf{y}. \quad (10)$$

The main problem in the proposed algorithm is the determination of the maximum $\Delta \bar{\mathbf{y}}$, and minimum, since the function $\bar{\mathbf{y}}$ is not known in advance. In the course of repeated trial calculations and analysis of experimental data, it was found that the initial data $\bar{\mathbf{y}}$ and $\Delta \mathbf{y}$ after filtering by standard methods, for example, using wavelets, can be used as the first iterations of the algorithm. At further iterations of the algorithm, the found sequence can already be used. At further iterations of the algorithm, the found sequence $\bar{\mathbf{y}}$ can be used.

3.2. Pulse triad filtering and analysis

Filtering the triad of impulses (loading, reflected and transmitted) is complicated by the presence of interrelations between them, such as the law of conservation of energy and momentum. Therefore, it is necessary to solve the problem of filtering these signals in a consistent manner and introduce the following additional restrictions into problems (1) and (2):

$$\bar{y}_{Ld}(t) - \bar{y}_{Tr}(t) - \bar{y}_{Rf}(t) \geq 0, \quad (11)$$

where $\bar{y}_{Ld}, \bar{y}_{Rf}, \bar{y}_{Tr}$ are the clearance values of the loading, reflected and transmitted pulses, respectively. For a discrete description, we represent $\bar{y}_{Ld}, \bar{y}_{Rf}, \bar{y}_{Tr}$ as lattice functions in the form of a sequence of readings $\bar{y}_{Ld}, \bar{y}_{Rf}$ and \bar{y}_{Tr} . Then Eq. (11) has the following form:

$$\bar{y}_{Ld}[k] - \bar{y}_{Tr}[k] - \bar{y}_{Rf}[k] \geq 0. \quad (12)$$

To filter the signals \mathbf{y}_{Ld} and \mathbf{y}_{Rf} , their descriptions in the form of Eqs. (9) and (10) can be used, however, \mathbf{y}_{Rf} has a more complex structure, and it is advisable to process the sum of the signals $\mathbf{y}_{Rf} + \mathbf{y}_{Tr}$, the form of which is similar to \mathbf{y}_{Ld} . Then the task of filtering the triad \mathbf{y}_{Ld} , \mathbf{y}_{Tr} and \mathbf{y}_{Rf} is formulated as follows:

$$J = \min_{\bar{y}_{Ld}, \bar{y}_{Tr}, \bar{y}_{Rf}} \left\{ \int_{t_0}^{t_k} (\mathbf{y}_{Ld} - \bar{y}_{Ld})^2 dt + \int_{t_0}^{t_k} \left(\frac{d\mathbf{y}_{Ld}}{dt} - \frac{d\bar{y}_{Ld}}{dt} \right)^2 dt + \int_{t_0}^{t_k} (\mathbf{y}_{Tr} - \bar{y}_{Tr})^2 dt + \int_{t_0}^{t_k} \left(\frac{d\mathbf{y}_{Tr}}{dt} - \frac{d\bar{y}_{Tr}}{dt} \right)^2 dt + \int_{t_0}^{t_k} (\mathbf{y}_{Rf} - \bar{y}_{Rf})^2 dt + \int_{t_0}^{t_k} \left(\frac{d\mathbf{y}_{Rf}}{dt} - \frac{d\bar{y}_{Rf}}{dt} \right)^2 dt \right\}, \quad (13)$$

with restrictions,

$$\begin{aligned} \frac{d^2}{dt^2} \bar{y}_{Ld} &\geq 0, t \in \left[t_0, t_{\max\left(\frac{d\bar{y}_{Ld}}{dt}\right)} \right], \frac{d^2}{dt^2} \bar{y}_{Ld} \leq 0, t \in \left[t_{\max\left(\frac{d\bar{y}_{Ld}}{dt}\right)}, t_{\min\left(\frac{d\bar{y}_{Ld}}{dt}\right)} \right], \\ \frac{d^2}{dt^2} \bar{y}_{Ld} &\geq 0, t \in \left[t_{\min\left(\frac{d\bar{y}_{Ld}}{dt}\right)}, t_k \right], \frac{d^2}{dt^2} \bar{y}_{Tr} \geq 0, t \in \left[t_0, t_{\max\left(\frac{d\bar{y}_{Tr}}{dt}\right)} \right], \\ \frac{d^2}{dt^2} \bar{y}_{Tr} &\leq 0, t \in \left[t_{\max\left(\frac{d\bar{y}_{Tr}}{dt}\right)}, t_{\min\left(\frac{d\bar{y}_{Tr}}{dt}\right)} \right], \frac{d^2}{dt^2} \bar{y}_{Tr} \geq 0, t \in \left[t_{\min\left(\frac{d\bar{y}_{Tr}}{dt}\right)}, t_k \right], \\ \frac{d^2}{dt^2} (\bar{y}_{Rf} + \bar{y}_{Tr}) &\geq 0, t \in \left[t_0, t_{\max\left(\frac{d(\bar{y}_{Rf} + \bar{y}_{Tr})}{dt}\right)} \right], \frac{d^2}{dt^2} \bar{y}_{Rf} \leq 0, \\ t \in \left[t_{\max\left(\frac{d(\bar{y}_{Rf} + \bar{y}_{Tr})}{dt}\right)}, t_{\min\left(\frac{d(\bar{y}_{Rf} + \bar{y}_{Tr})}{dt}\right)} \right], \frac{d^2}{dt^2} (\bar{y}_{Rf} + \bar{y}_{Tr}) &\geq 0, t \in \left[t_{\min\left(\frac{d(\bar{y}_{Rf} + \bar{y}_{Tr})}{dt}\right)}, t_k \right], \\ \bar{y}_{Ld}(t) - \bar{y}_{Tr}(t) - \bar{y}_{Rf}(t) &\geq 0. \end{aligned}$$

Using expression (13), one can obtain:

$$\begin{aligned} J = \min_{\bar{y}_{Ld}, \bar{y}_{Tr}, \bar{y}_{Rf}} \left\{ (\mathbf{y}_{Ld} - \bar{y}_{Ld})^T (\mathbf{y}_{Ld} - \bar{y}_{Ld}) + (\Delta \mathbf{y}_{Ld} - \Delta \bar{y}_{Ld})^T (\Delta \mathbf{y}_{Ld} - \Delta \bar{y}_{Ld}) + \right. \\ \left. + (\mathbf{y}_{Tr} - \bar{y}_{Tr})^T (\mathbf{y}_{Tr} - \bar{y}_{Tr}) + (\Delta \mathbf{y}_{Tr} - \Delta \bar{y}_{Tr})^T (\Delta \mathbf{y}_{Tr} - \Delta \bar{y}_{Tr}) + \right. \\ \left. + (\mathbf{y}_{Rf} - \bar{y}_{Rf})^T (\mathbf{y}_{Rf} - \bar{y}_{Rf}) + (\Delta \mathbf{y}_{Rf} - \Delta \bar{y}_{Rf})^T (\Delta \mathbf{y}_{Rf} - \Delta \bar{y}_{Rf}) \right\}. \quad (14) \end{aligned}$$

Using the properties of finite differences (4) and introducing new variables:

$$\mathbf{x} = \begin{bmatrix} \mathbf{x}_{Ld} \\ \mathbf{x}_{Tr} \\ \mathbf{x}_{Rf} \end{bmatrix} = \begin{bmatrix} \mathbf{y}_{Ld} - \bar{y}_{Ld} \\ \mathbf{y}_{Tr} - \bar{y}_{Tr} \\ \mathbf{y}_{Rf} - \bar{y}_{Rf} \end{bmatrix}, \quad (15)$$

We can simplify Eq. (14) as follows:

$$\begin{aligned} J = \min_{\bar{y}_{Ld}, \bar{y}_{Tr}, \bar{y}_{Rf}} \left\{ \mathbf{x}_{Ld}^T \mathbf{x}_{Ld} + \mathbf{x}_{Ld}^T \mathbf{H}_1^T \mathbf{H}_1 \mathbf{x}_{Ld} + \mathbf{x}_{Tr}^T \mathbf{x}_{Tr} + \right. \\ \left. + \mathbf{x}_{Tr}^T \mathbf{H}_1^T \mathbf{H}_1 \mathbf{x}_{Tr} + \mathbf{x}_{Rf}^T \mathbf{x}_{Rf} + \mathbf{x}_{Rf}^T \mathbf{H}_1^T \mathbf{H}_1 \mathbf{x}_{Rf} \right\} = \\ = \min_{\bar{y}_{Ld}, \bar{y}_{Tr}, \bar{y}_{Rf}} \left\{ \mathbf{x}^T \mathbf{H} \mathbf{x} \right\}, \quad (16) \\ \mathbf{H} = \begin{bmatrix} \mathbf{I} + \mathbf{H}_1^T \mathbf{H}_1 & 0 & 0 \\ 0 & \mathbf{I} + \mathbf{H}_1^T \mathbf{H}_1 & 0 \\ 0 & 0 & \mathbf{I} + \mathbf{H}_1^T \mathbf{H}_1 \end{bmatrix}. \end{aligned}$$



$$J = \min_{\tau_{Tr}, \tau_{Rf}} \left\{ \Phi(\tau_{Tr}, \tau_{Rf}) \right\}, \quad (21)$$

with constraints: $\tau_{\min} \leq \tau_{Tr} \leq \tau_{\max}, \tau_{\min} \leq \tau_{Rf} \leq \tau_{\max}$, where $\Phi(\tau_n, \tau_o)$ is a function calculated as a solution to the quadratic programming problem, similar to Eq. (19) for fixed τ_o and τ_p :

$$\Phi(\tau_n, \tau_o) = \min_{\bar{y}_n, \bar{y}_o, \bar{y}_c} \left\{ \mathbf{x}[\tau_n, \tau_o]^T \mathbf{H} \mathbf{x}[\tau_n, \tau_o] \right\}, \quad (22)$$

with constraints: $\Lambda \mathbf{x}[\tau_{Tr}, \tau_{Rf}] \geq \Lambda \mathbf{y}[\tau_{Tr}, \tau_{Rf}]$, where:

$$\mathbf{x}[\tau_{Tr}, \tau_{Rf}] = \begin{bmatrix} \mathbf{x}_{Ld} \\ \mathbf{x}_{Tr}[\tau_{Tr}] \\ \mathbf{x}_{Rf}[\tau_{Rf}] \end{bmatrix} = \begin{bmatrix} \mathbf{y}_{Ld} - \bar{\mathbf{y}}_{Ld} \\ \mathbf{y}_{Tr}[\tau_{Tr}] - \bar{\mathbf{y}}_{Tr} \\ \mathbf{y}_{Rf}[\tau_{Rf}] - \bar{\mathbf{y}}_{Rf} \end{bmatrix} = \begin{bmatrix} \mathbf{y}_{Ld} - \bar{\mathbf{y}}_{Ld} \\ \mathbf{A}^{\tau_{Tr}} \mathbf{y}_{Tr} - \bar{\mathbf{y}}_{Tr} \\ \mathbf{A}^{\tau_{Rf}} \mathbf{y}_{Rf} - \bar{\mathbf{y}}_{Rf} \end{bmatrix}, \mathbf{y}[\tau_{Tr}, \tau_{Rf}] = \begin{bmatrix} \mathbf{y}_{Ld} \\ \mathbf{A}^{\tau_{Tr}} \mathbf{y}_{Tr} \\ \mathbf{A}^{\tau_{Rf}} \mathbf{y}_{Rf} \end{bmatrix}. \quad (23)$$

Using the algorithm described above, we processed the obtained experimental data.

An analysis of the signals showed that the oscillatory components characterizing the second and subsequent maxima on the transmitted pulse are also present in the loading pulse. These components can be attributed to the noise of the experimental setup itself, and, as a result, can be removed and not taken into account in methods for calculating the characteristics of materials (see Fig. 4).

4. The Ice Model

In this work, we include micromechanics in the model of dynamic deformation. Therefore, we use the problem of propagating a steady elasto-plastic wave as a test problem. Such a problem is frequently used for a model verification of the constitutive equations of a medium (see [47]). In this paper we propose a model for the propagation of steady elastoplastic wave based on the dynamics of dislocations. In this model we take into account additional relaxation caused by the variation in the so-called mass-velocity of ice particles.

From the experiments with other ice materials, it was found that the shock front in the structural nonuniform medium represents the superposition of two modes of motion. The first is the average motion of the flat front and the second mode is the quickly fluctuating motion of certain parts with respect to the average motion of the front (see [47]). In this case, the real carriers of plastic deformation (such as dislocations) cannot be exactly determined. As the authors of [47] wrote, "the only fact that can be estimated using the interferometric methods of detection of wave processes is the spatial scale of the correlation motion of deformation carriers, which looks like the ice particle velocity pulsation at the mesolevel". We assume that the same physical mechanisms are present during impact, such as the like loading of ice.

The model of ice behavior during uniaxial deformation at a high strain rate is as follows. Ice material behavior is represented in the form of interacting subsystems, the first of which determines the dislocation mechanism of deformation, studied in detail in [48-53], and the second determines the dissipative properties of the material. It is assumed that, at given loading rates, a stationary front of plastic deformation is formed, and the dispersion of strain rates is due to the dissipative properties of the medium in which the plastic front moves. Depending on the parameters of the experiments (temperature and speed of the impactor), different sequences of plastic deformation processes are assumed, which are expressed in the interaction of the introduced subsystems, so they can be connected in series in a different order, or in parallel in the case of a superposition of deformations of these subsystems.

We consider the deformation of ice in the temperature range from -10°C to -20°C only.

To describe the first subsystem, which corresponds to the passage of the plastic front, a model of the dislocation dynamics is used.

For our ice samples we assume that: $\epsilon_{11}^p + \epsilon_{22}^p + \epsilon_{33}^p = 0$.

The relation between the normal stress σ , total deformation ϵ_t , and plastic deformation ϵ^p is given by [52, 53]:

$$\sigma - \rho c_l^2 \epsilon_t = -2\mu \epsilon^p, \quad (24)$$

where $c_l = \sqrt{(\lambda + 2\mu) / \rho}$ is the longitudinal sound velocity.

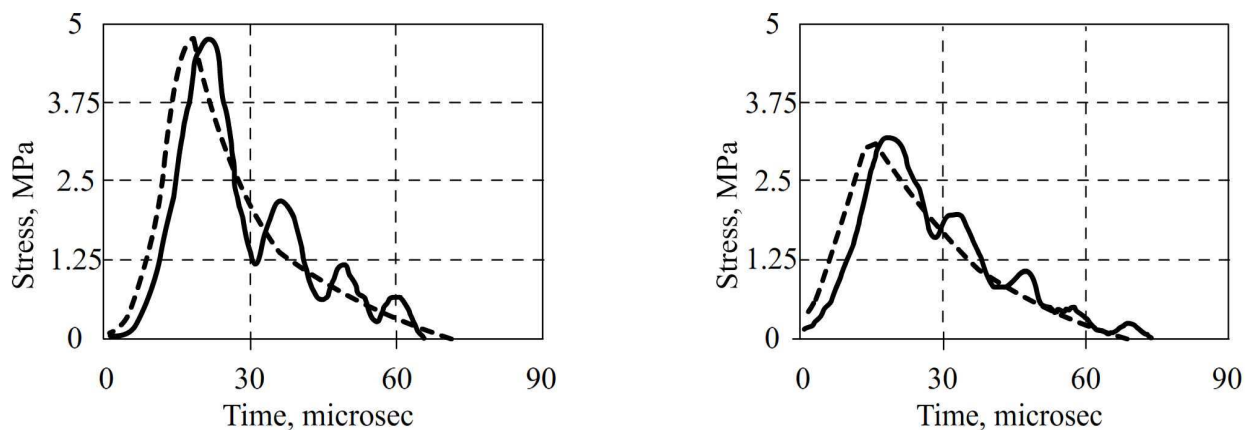


Fig. 4. Signal processing results; The solid line indicates the original signal, and the dashed line shows the signal after filtering.



The governing relation for one-dimensional wave propagation is introduced as follows:

$$\sigma_t - \rho c_1^2 \varepsilon_t = -\frac{8}{3} \gamma_t^p, \quad (25)$$

$$\gamma^p = \frac{1}{2} (\varepsilon_{11}^p - \varepsilon_{22}^p), \quad (26)$$

where γ^p is the shear plastic strain and t is time.

The shear strain rate can be represented as follows $\gamma_t^p = b N_m V_d$, where γ_t^p is the shear strain rate, N_m is the dislocation density, V_d is the dislocation velocity, and b is the magnitude of the Burgers vector.

The dislocation density can be represented as ([49]):

$$N_m = N_{m0} + \alpha \gamma^p, \quad (27)$$

where N_{m0} is the initial dislocation density and α is the coefficient of dislocation multiplication.

The following formula for the dislocation velocity is valid in this case:

$$V_d = \frac{b(\tau - \tau_0)}{B}, \quad (28)$$

where B is the dislocation viscosity, τ is the shear stress, and τ_0 is the reverse stress. Then the governing equation (25) obtains the following form:

$$\sigma_t - \rho c_1^2 \varepsilon_t = \gamma_* \mu (1 - M \gamma^p) (\tau - \tau_0), \quad (29)$$

where,

$$\gamma_* = \frac{b^2 N_{m0}}{B}, \quad M = \frac{\alpha}{N_{m0}}, \quad \tau_* = \tau_0 / \mu. \quad (30)$$

Equation (30) can be represented as follows:

$$\gamma_t^p = \gamma_* \mu (1 + M \gamma^p) [(\varepsilon - 2\gamma^p) - \tau_*]. \quad (31)$$

Considering the mass and momentum balance equations:

$$\rho u_t + \sigma_x = 0, \quad (32)$$

$$u_x + \varepsilon_t = 0, \quad (33)$$

and Eq. (30) one can obtain the system of equations for the dynamic deformation of a one-dimensional isotropic material. In Eqs. (32) and (33) u is the ice particle mass-velocity [54].

Let us consider the propagation of a stationary wave with the constant velocity c_0 . Then we can introduce the variable $z = x - c_0 t$ and rewrite the set of equations in the following form:

$$\begin{aligned} \rho c_0 u_z - \sigma_z &= 0, \\ c_0 \varepsilon_z - u_z &= 0, \\ c_0 \gamma_z^p &= \gamma_* \mu (1 + M \gamma^p) [(\varepsilon - 2\gamma^p) - \tau_*] \end{aligned} \quad (34)$$

We can rewrite system (34) and obtain the equation with respect to the particle velocity u :

$$u_z + L_1 u + L_2 u^2 + L_3 = 0, \quad (35)$$

where,

$$L_1 = \frac{1}{c_0} \gamma_* \mu (a - 2 - M \tau_*), \quad L_2 = \frac{\gamma_* \mu M}{a c_0^2} (a - 2), \quad L_3 = a \gamma_* \mu \tau_*, \quad a = \frac{8\mu}{3} \frac{1}{\rho(c_1^2 - c_0^2)}. \quad (36)$$

The solution of Eq. (35) has the following form:

$$u = u_0 \left\{ 1 + \exp \left[\frac{u_0 \gamma_* M (a - 2)}{a c_0} z \right] \right\}^{-1}, \quad (37)$$

where u_0 is the value of the particle velocity at $z = -\infty$. Formula (37) corresponds to the propagation of the stationary wave front from $z = -\infty$ to $z = +\infty$. The wave slope is determined by the dislocation parameters. Using data from [46-51], one can calculate the shock wave profile. This profile is presented in Fig. 5.

This profile does not consider that the propagation of a shock front is certainly nonuniform in the velocity space process. Therefore, we can expect that the real response under shock loading cannot be described exactly as such.

To take into account the dissipative effects we assume that the front generated by the dislocation mechanism acts on the second subsystem. This mechanism gives us the following equation:

$$E \frac{\partial^2 v}{\partial x^2} - Q_1 - Q_2(u) = \rho \frac{\partial^2 v}{\partial t^2}, \quad (38)$$



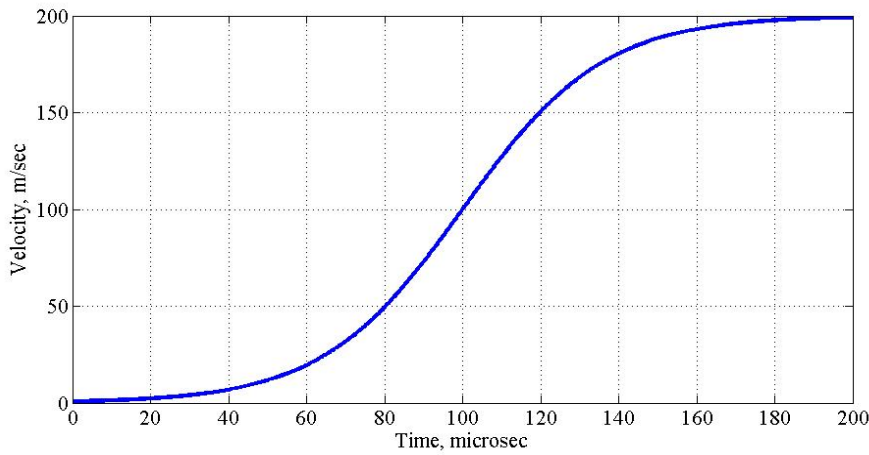


Fig. 5. Shock wave profile.

where E is the Young modulus, ρ is the initial ice density, Q_1 is the force of internal interaction, $Q_2(u)$ is the force as a result of the action of the first subsystem, and v is the ice particle displacement.

By analogy with the well-known solution of the wave operator, one can obtain the following expressions for deformation and equation, which relates the mass-velocity of ice particles in the form:

$$\varepsilon = \frac{v_t}{c_0}, \quad v_{tt} + \phi_1 v_t = \phi_2 u, \tag{39}$$

where ϕ_1 is the coefficient of internal viscosity and ϕ_2 is the coefficient. As before we introduce the variable z , and then Eq. (39) becomes:

$$\begin{aligned} c_0^2 v_{zz} &= v_{tt}, & -c_0 v_z &= v_t, \\ v_{zz} - \frac{\phi_1}{c_0} v_z &= \frac{\phi_2}{c_0^2} u, \\ \varepsilon(z) &= -v_z, \end{aligned} \tag{40}$$

Then we have:

$$\begin{aligned} \varepsilon_z - \frac{\phi_1}{c_0} \varepsilon &= -\frac{\phi_2}{c_0^2} u = \frac{b_1}{e^{a_1 z} + 1}, \\ a_1 &= \frac{u_0 \gamma_* M(a-2)}{ac_0}, \quad a_2 = -\frac{\phi_1}{c_0}, \quad b_1 = -\frac{\phi_2 u_0}{c_0^2}. \end{aligned} \tag{41}$$

The solution of Eq. (41) can be obtained as follows:

$$\begin{aligned} \varepsilon_z + a_2 \varepsilon &= \frac{b_1}{e^{a_1 z} + 1}, \\ \varepsilon &= \int_{-\infty}^z \frac{b_1 e^{-a_2(z-\xi)}}{e^{a_1 \xi} + 1} d\xi = \int_{-\infty}^z \frac{b_1 e^{-a_2 z + a_2 \xi}}{e^{a_1 \xi} + 1} d\xi = b_1 e^{-a_2 z} \int_{-\infty}^z \frac{e^{a_2 \xi}}{e^{a_1 \xi} + 1} d\xi, \\ s(\xi) &= e^{a_1 \xi}, \\ \varepsilon &= b_1 e^{-a_2 z} \int_{-\infty}^z \frac{s^{a_2} ds}{s+1} = b_1 e^{-a_2 z} \int_{-\infty}^z \frac{s^{a_2-1} ds}{s+1} = \frac{b_1}{a_1} e^{-a_2 z} \int_{s(-\infty)}^{s(z)} \frac{ds}{s^{a_2+1} (s+1)}, \\ \chi &= -\frac{a_2}{a_1}, \\ \varepsilon &= \frac{b_1}{a_1} e^{-a_2 z} \int_{s(-\infty)}^{s(z)} \frac{ds}{s^{\chi+1} (s+1)} = \frac{b_1}{a_1} e^{-a_2 z} \left[s^{-\chi} \Phi(-s, 1, -\chi) \Big|_{s(-\infty)}^{s(z)} \right] = \\ &= \frac{b_1}{a_1} e^{-a_2 z} \left[s(z)^{-\chi} \Phi(-s(z), 1, -\chi) - s(-\infty)^{-\chi} \Phi(-s(-\infty), 1, -\chi) \right], \end{aligned} \tag{42}$$

where $\Phi(\dots)$ is the Lerch function.

The total force acting on ice during impact loading is as follows: $Q = Q_1 + Q_2(u)$.

Let us relate this force to the ice deformation using Eq. (39):

$$\begin{aligned} \varepsilon &= \frac{v_t}{c_0}, \quad v_{tt} + \phi_1 v_t = \phi_2 u, \\ v_{tt} &= -\phi_1 v_t + \phi_2 u = -Q = -\phi_1 c_0 \varepsilon + \phi_2 u, \end{aligned}$$



Then we rewrite these expressions via the variable z as follows:

$$\begin{aligned}
 c_0^2 v_{zz} &= v_{tt}, \quad -c_0 v_z = v_t, \\
 v_{zz} &= \frac{\phi_1}{c_0} v_z + \frac{\phi_2}{c_0^2} u = -Q = -\frac{\phi_1}{c_0} \varepsilon(z) + \frac{\phi_2}{c_0^2} u, \\
 Q &= \frac{\phi_1}{c_0} \varepsilon(z) - \frac{\phi_2}{c_0^2} u = \frac{\phi_1}{c_0} \varepsilon(z) - \frac{\frac{\phi_2}{c_0^2} u_0}{1 + \exp\left[\frac{u_0 \gamma_s M(a-2)}{ac_0} z\right]}.
 \end{aligned}
 \tag{43}$$

This force can be measured in experimentally and has the following form:

$$Q(t) = a_1 t + \frac{a_2}{1 + \exp(a_3 t - a_3 a_4)} - \frac{a_2}{1 + \exp(-a_3 a_4)},
 \tag{44}$$

where a_1, a_2, a_3 and a_4 are the approximation parameters. To estimate the coefficients in Eq. (44), we can use the methods of parametrical identification.

In terms of optimization this problem can be described as follows:

$$J = \min_{a_i} \left\{ \sum_{k=0}^N [Q^*(t_k) - Q(t_k)]^2 \right\},
 \tag{45}$$

where J is the functional, $Q^*(t_k)$ is the magnitude of the force measured at time t_k , $Q(t_k)$ is the magnitude of the force computed according to expression (44) at time t_k , and N is the sample size.

The algorithm of analysis and filtering of the experimental data described in section 3 has been modified and applied at the stage of signal preprocessing to exclude the influence of multiplicative and additive noise. This method increases the stability of solving the problem of estimating parameters in model (45) using the Levenberg–Marquardt algorithm [53].

When the loading rate increase, it leads to a change in the sequence of subsystems in the material model, now the dissipative part is switched on first, and only then the dislocation fracture mechanism appears. Then, the model obtains the following form:

$$\begin{aligned}
 v_z &= u_z - L_1 u + L_2 u^2 \\
 v_{zz} &= \frac{\phi_1}{c_0} v_z,
 \end{aligned}
 \tag{46}$$

under appropriate initial conditions. By integrating the second equation in (46), one obtains $v_z = a_0 e^{-a_2 z} = y$. Substituting the solution of the linear equation into the first equation (46), one obtains the general Riccati equation:

$$u_z - L_1 u + L_2 u^2 = a_0 e^{-a_2 z}.
 \tag{47}$$

After some manipulation, we can obtain the modified Bessel equation:

$$\begin{aligned}
 I &= e^{L_2 \int u dz}, \quad I_{zz} - L_1 I_z - L_2 a_0 e^{-a_2 z} I = 0, \\
 s &= e^{-\frac{a_2}{2} z}, \quad s^2 I_{ss} + \left[1 + \frac{2L_1}{a_2}\right] s I_s - \frac{4L_2 a_0}{a_2^2} s^2 I = 0, \\
 \xi &= \frac{2\sqrt{L_2 a_0}}{a_2} s, \quad \xi^2 I_{\xi\xi} + \xi \frac{a_2 + 2L_1}{a_2} I_\xi - \xi^2 I = 0, \\
 I &= \xi^{-\frac{L_1}{a_2}} y, \quad \xi^2 y_{\xi\xi} + \xi y_\xi - \left[\xi^2 + \frac{L_1^2}{a_2^2}\right] y = 0.
 \end{aligned}
 \tag{48}$$

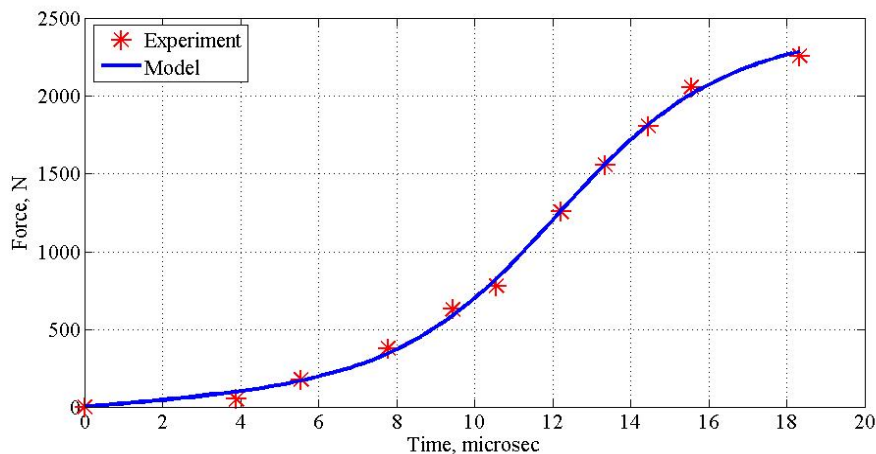


Fig. 6. Force profile for ice describing the elastic and plastic deformation mechanism for a strain rate of $1.4 \cdot 10^3 \text{ s}^{-1}$.



The solution of Eq. (48) is determined by the following expression:

$$I = e^{L_2 \int u dz} = \left(\frac{2\sqrt{L_2 a_0}}{a_2} \right)^{-\frac{L_1}{a_2}} e^{\frac{L_1 z}{2}} H \left(\left(\frac{2\sqrt{L_2 a_0}}{a_2} \right)^{-\frac{L_1}{a_2}} e^{\frac{L_1 z}{2}} \right), \quad (49)$$

$$\int u dz = \frac{1}{L_2} \ln I, \quad u = \frac{I_z}{L_2 I},$$

where $H(\dots)$ is the general solution of the modified Bessel equation.

The equation for the force measured during the experiment is defined as follows:

$$\varepsilon = \frac{u}{c_0}, \quad Q_{sp.} = C_{sp.} \varepsilon = C_{sp.} \frac{u}{c_0}. \quad (50)$$

To estimate the coefficients of the models of the first and second modes, based on the experimental data, parametric identification methods are used. Finally, the profile of the force $Q(t)$ is calculated and drawn in Fig. 5. In the same figure asterisks represent the experimental results. There are slight differences in the values calculated according to the proposed model and test results. For a constant strain rate, the following results were obtained:

$$a_1 = 18.3125$$

$$a_2 = 2.0435e+003$$

$$a_3 = -0.5026$$

$$a_4 = 12.13091.$$

The profile of the force $Q(t)$ is shown in Fig. 6.

5. Conclusions and Discussion

To determine the mechanical properties of ice at high-strain rates the Kolsky method was used at a strain rate of $1.4 \cdot 10^3 \text{ s}^{-1}$. A new procedural approach and experimental data filtration algorithm were suggested. An ice phenomenological model was proposed that makes it possible to obtain a relationship between the measured force and the parameters of the material and loading modes. The verification of the model was carried out according to the results of experiments, during which the forces were obtained in the study of the destruction of ice samples for high strain rates. The analytical force model describes the experimental data well. The process of identifying the parameters of the force model using the least squares method was proposed. Future studies should identify the model of ice deformation and destruction by determining of the coefficients of ice characteristics and loading parameters, taking into account the physical justification of the processes occurring in the samples in more detail.

Processing data obtained in the experiment the authors initially used different methods of analyses and filtering of the signal including wavelets, various types of filters, and analysis in the frequency domain. Those methods significantly distort the signal and cause the loss of its physical properties. Oscillations visible in Fig. 2 have the same frequency range as the signal front. Therefore, the removal of these components by standard methods leads to the signal front flattening and affects significantly the characteristics (for example the incubation time) describing the material destruction. It signifies the necessity to maintain the physical validity of signal characteristics resulted from the processing. The second issue is coordinated analysis and filtering of all three signals obtained in the experiment. The relation of the momentum conservation law in the experiment should be satisfied. It is impossible to achieve that requirement using standard methods. The frequency domain filtering introduces a phase shift into the signal, and it is very difficult to control the value of that shift, but it changes the signal maximum peak time. That is, our goal is to propose a co-filtering algorithm for three impulses without losing the front slope of all three signals and to satisfy the momentum conservation law. The obtained algorithm is reduced to a quadratic programming problem, which can be efficiently implemented using computer technology. The complexity of implementation is comparable to that of other filtering methods when choosing the appropriate parameters of classical filters or decompositions with high accuracy.

The research reveals that the stand recording equipment introduces the uncontrolled shift into the recorded data in the time domain. Those shifts result in the failure of the momentum conservation law. There is another problem. Analysis of characteristics determining the destruction moment requires their strict binding to the time axis, and uncontrolled phase shifts are sources of errors in determining that moment of destruction. The phase shifts have a systematic component and a random component. The determination of the shifts must be systematic and performed for all three impulses simultaneously, taking into account the momentum conservation law. Thus, the correlation methods, as a proposed alternative, do not take into account the momentum conservation law. The correlation methods require a reference signal, but the resulting signal profiles are unique in each experiment. Therefore, it is not possible to predict the ideal signal for each experiment. The authors of the paper propose the algorithm that allows including other restrictions related to the physics of the fracture process. Research in this area is ongoing.

Our goal is to perform filtering without distorting the steepness signal profile and determine the true position of the maximum, taking into account the physics of the destruction process. Therefore, the given characteristics of the destruction process have already taken into account the time shift of the curves introduced by the measuring system of the stand. Taken into account the errors (time shifts) of the measuring systems increases the accuracy of determining the characteristics of the material.

Author Contributions

A. Kuchmin: Methodology, experiment, computations. A. Abramyan: Conceptualization, formal analysis, writing, derivations. A. Abramyan and A. Kuchmin: Discussion of the results, editing the manuscript. All authors have read and agreed to the published version of the manuscript.

Acknowledgments

The work was carried out within the framework of the state assignment of the Ministry of Science and Higher Education of the Russian Federation for the Institute of Problems in Mechanical Engineering of the Russian Academy of Sciences.



Conflict of interest

The authors declared no potential conflicts of interest concerning the research, authorship, or publication of this article.

Funding

The work was carried out within the framework of the state assignment of the Ministry of Science and Higher Education of the Russian Federation for the Institute of Problems in Mechanical Engineering of the Russian Academy of Sciences.

Data availability statements

The datasets generated and/or analyzed during the current study are available from the corresponding author upon reasonable request.


References


- [1] Jones, S.J., A review of the strength of iceberg and other freshwater ice and the effect of temperature, *Cold Regions Science and Technology*, 47, 2007, 256–262.
- [2] Michel, B., *Ice Mechanics*, University of Laval Press: Quebec, QC, Canada, 1978.
- [3] Dempsey, J.P., Research trends in ice mechanics, *International Journal of Solids and Structures*, 37, 2000, 131–153.
- [4] Cole, D.M., The microstructure of ice and its influence on mechanical properties, *Engineering Fracture Mechanics*, 68, 2001, 1797–1822.
- [5] Schulson, E.M., Duval, P., *Creep and Fracture of Ice*, Cambridge University Press, Cambridge, UK, 2009.
- [6] Lister, G.S., Hobbs, B.E., The simulation of fabric development during plastic deformation and its application to quartzite: the influence of deformation history, *Journal of Structural Geology*, 2, 1980, 355–370.
- [7] Jones, S.J., High strain-rate compression tests on ice, *Journal of Physical Chemistry*, 101, 1997, 6099–6101.
- [8] Flegel, A.B., Ice-crystal icing investigation on a Honeywell Uncertified Research Engine in an altitude simulation icing facility, *Journal of Turbomachinery*, 143, 2021, 101002.
- [9] Trontin, P., Villedieu, P., A comprehensive accretion model for glaciated icing conditions, *International Journal of Multiphase Flow*, 108, 2018, 105–123.
- [10] Baumert, A., Bansmer, S., Trontin, P., Villedieu, P., Experimental and numerical investigations on aircraft icing at mixed phase conditions, *International Journal of Heat and Mass Transfer*, 123, 2018, 957–978.
- [11] Norde, E., Van Der Weide, E.T.A., Hoijmakers, H.W.M., Eulerian method for ice crystal icing, *AIAA Journal*, 56, 2018, 222–234.
- [12] Amelyushkin, I.A., Stasenko, A.L., Simulation of the interaction of ice crystals with the surface of a flying vehicle, *Journal of Engineering Physics and Thermophysics*, 93, 2020, 576–584.
- [13] Senoner, J.-M., Trontin, P., Reitter, L.M., Karpen, N., Schremb, M., Vargas, M., Villedieu, P., Ice particle impact on solid walls: Size modeling of reemitted fragments, *International Journal of Impact Engineering*, 169, 2022, 104322.
- [14] Roisman, I.V., Tropea, C., Impact of a crushing ice particle onto a dry solid wall, *Proceedings of the Royal Society A*, 471, 2015, 20150525.
- [15] Meglis, I., Jordana, I., High Speed Testing of Freshwater Granular Ice, Technical Report, National Research Council Canada, Institute for Marine Dynamics: St. John's, NL, Canada, 1998.
- [16] Hauk, T., Bonaccorso, E., Roisman, I.V., Tropea, C., Ice crystal impact onto a dry solid wall. Particle fragmentation, *Proceedings of the Royal Society A*, 471, 2015, 20150399.
- [17] Burke, S.E., Miller, M.E., Continetti, R.E., Velocity dependence of submicron ice grain rebound, sticking, particle fragmentation, and impact ionization up to 2.4 km/s, *ACS Earth and Space Chemistry*, 7, 2023, 764–773.
- [18] Miller, M.E.C., Burke, S.E., Continetti, R.E., Production and impact characterization of enceladus ice grain analogues, *ACS Earth and Space Chemistry*, 6, 2022, 1813–1822.
- [19] Jiang, H., Wang, H., Scott, V., Li, B., Numerical analysis of oblique hypervelocity impact damage to space structural materials by ice particles in cryogenic environment, *Acta Astronautica*, 195, 2022, 392–404.
- [20] Chen, S., Gad, E., Zhang, L., Lam, N., Xu, S., Lu, G., Experiments on an ice ball impacting onto a rigid target, *International Journal of Impact Engineering*, 167, 2022, 104281.
- [21] Roisman, I.V., Hydrodynamic model of a collision of a spherical plastic ice particle with a perfectly rigid substrate, *International Journal of Impact Engineering*, 159, 2022, 104019.
- [22] Senoner, J.-M., Trontin, P., Reitter, L.M., Karpen, N., Schremb, M., Vargas, M., Villedieu, P., Ice particle impact on solid walls: Size modeling of reemitted fragments, *International Journal of Impact Engineering*, 169, 2022, 104322.
- [23] Reitter, L.M., Lohmann, H., Schremb, M., Roisman, I.V., Hussong, J., Tropea, C., Impact of an ice particle onto a dry rigid substrate: Dynamic sintering of a residual ice cone, *Cold Regions Science and Technology*, 194, 2022, 103416.
- [24] Zhu, Z., Kang, G., Ma, Y., Xie, Q., Zhang, D., Ning, J., Temperature damage and constitutive model of frozen soil under dynamic loading, *Mechanics of Materials*, 102, 2016, 108–116.
- [25] Zhu, Z., Cao, C., Fu, T. SHPB test analysis and a constitutive model for frozen soil under multiaxial loading, *International Journal of Damage Mechanics*, 29, 2020, 626–645.
- [26] Zhu, Z., Fu, T., Ning, J., Li, B., Mechanical behavior and constitutive model of frozen soil subjected to cyclic impact loading, *International Journal of Impact Engineering*, 177, 2023, 104531.
- [27] Weng, L., Wu, Z., Liu, Q., Dynamic mechanical properties of dry and water-saturated siltstones under sub-zero temperatures, *Rock Mechanics and Rock Engineering*, 53, 2020, 4381–4401.
- [28] Weinberg, K., Khosravani, M.R., Thimm, B., Reppel, T., Bogunia, L., Aghayan, S., Nötzel, R., Hopkinson bar experiments as a method to determine impact properties of brittle and ductile materials, *GAMM Mitteilungen*, 41, 2018, e201800008.
- [29] Nakao, Y., Yamada, H., Ogasawara, N., Matsuzawa, T., Impact compression test of ice by combining SHPB method and high-speed camera observation, *Experimental Mechanics*, 62, 2022, 1227–1240.
- [30] Song, Z., Wang, Z., Kim, H., Ma, H., Pulse shaper and dynamic compressive property investigation on ice using a large-sized modified split Hopkinson pressure bar, *Latin American Journal of Solids and Structures*, 13, 2016, 391–406.
- [31] Li, S., Feng, X., Xie, R., Zhang, F., Hu, W., Xu, W., Huang X., Dynamic compression property of distill-water ice and impurity-water ice at high strain rates, *Baozha Yu Chongji/Explosion and Shock Waves*, 39, 2019, 093103.
- [32] Isakov, M., Lange, J., Kilchert, S., May, M., In-situ damage evaluation of pure ice under high rate compressive loading, *Materials*, 12, 2019, 1236.
- [33] Wu, X., Prakash, V., Dynamic strength of distill water and lake water ice at high strain rates, *International Journal of Impact Engineering*, 76, 2015, 155–165.
- [34] Georges D., Saletti D., Montagnat M., Forquin P., Hagenmuller P., Influence of porosity on ice dynamic tensile behavior as assessed by spalling tests, *Journal of Dynamic Behavior of Materials*, 7, 2021, 575–590.
- [35] Saletti, D., Georges, D., Gouy, V., Montagnat, M., Forquin, P., A study of the mechanical response of polycrystalline ice subjected to dynamic tensile loading using the spalling test technique, *International Journal of Impact Engineering*, 132, 2019, 103315.
- [36] Zhang, Y., Wang, Q., Han, D., Xue, Y., Lu, S., Wang, P., Dynamic splitting tensile behaviours of distilled-water and river-water ice using a modified SHPB setup, *International Journal of Impact Engineering*, 145, 2020, 103686.
- [37] Zhang, Y., Wang, Q., Han, D., Xue, Y., Qu, J., Yao, H., Experimental study of the quasi-static and dynamic fracture toughness of freshwater ice using notched semi-circular bend method, *Engineering Fracture Mechanics*, 247, 2021, 107696.
- [38] Tang, E., Liu, C., Chang, M., Han, Y., Chen, C., Influence of freezing temperature and cotton content of ice on dynamic mechanical properties and energy dissipation, *The European Physical Journal Plus*, 137, 2022, 123.
- [39] Potter, R.S., Cammack, J.M., Braithwaite, C.H., Church, P.D., Walley, S.M., A study of the compressive mechanical properties of defect-free, porous and sintered water-ice at low and high strain rates, *Icarus*, 351, 2020, 113940.



- [40] Jones, S.J., Gagnon, R., Derradji, A., Bugden, A., Compressive strength of iceberg ice, *Canadian Journal of Physics*, 81, 2003, 191-200.
- [41] Dutta, P.K., Cole, D.M., Schulson, E.M., Sodhi, D.S., A fracture study of ice under high strain rate loading, *International Journal of Offshore and Polar Engineering*, 14, 2004, 182-188.
- [42] Kim, H., Keune, J.N., Compressive strength of ice at impact strain rates, *Journal of Materials Science*, 42, 2007, 2802.
- [43] Shazly, M., Prakash, V., Lerch, B.A., High strain-rate behavior of ice under uniaxial compression, *International Journal of Solids and Structures*, 46, 2009, 1499-1515.
- [44] Lian J., Ouyang Q., Zhao X., Liu F., Qi C., Uniaxial compressive strength and fracture mode of lake ice at moderate strain rates based on a digital speckle correlation method for deformation measurement, *Applied Sciences*, 7(5), 2017, 495.
- [45] Cole, D.M., Durell, G.D., A dislocation-based analysis of strain history effects in ice, *Philosophical Magazine A*, 81(7), 2001, 1849-1872.
- [46] Fukuda A., Shoji H., A dislocation model of the plastic deformation of single crystals of ice, *Cold Regions Science and Technology*, 4, 1981, 175-185.
- [47] Jones S.J., Gilra N.K., X-ray topographical study of dislocations in pure and HF-doped ice, *Philosophical Magazine*, 27, 1973, 457-472.
- [48] Louchet, F., From individual dislocation motion to collective behavior, *Journal of Materials Science*, 41, 2006, 2641-2646.
- [49] Shearwood, C., Whitworth R.W., The velocity of dislocations in crystals of HCl-doped ice, *Philosophical Magazine*, A65, 1992, 85-89.
- [50] Taupin, V., Varadhan, S., Chevy, J. et al., Effects of size on the dynamics of dislocations in ice single crystals, *Physical Review Letters*, 99, 2007, 155507-1-155507-4.
- [51] Taylor, J.W., Dislocation dynamics and dynamic yielding, *Journal of Applied Physics*, 36(10), 1965, 3146.
- [52] Duvall, G.E., *Propagation of Plane Shock Waves in a Stress Relaxing Medium*, Springer, Berlin, 1964.
- [53] Gill, P., Murray, W., Wright, M., *Practical Optimization*, Academic Press, London, 1981.
- [54] Indeitsev, D.A., Meshcheryakov, Y.I., Kuchmin, A.Y. et al., A multiscale model of propagation of steady elasto-plastic waves, *Doklady Physics*, 59, 2014, 423-426.

ORCID iD

Andrey Yu Kuchmin  <https://orcid.org/0000-0003-0699-6112>

Andrey K. Abramyan  <https://orcid.org/0000-0003-0576-8249>



© 2024 Shahid Chamran University of Ahvaz, Ahvaz, Iran. This article is an open access article distributed under the terms and conditions of the Creative Commons Attribution-NonCommercial 4.0 International (CC BY-NC 4.0 license) (<http://creativecommons.org/licenses/by-nc/4.0/>).

How to cite this article: Kuchmin A.Yu., Abramyan A.K. On the Problem of Modeling High Strain-Rate Behavior of Ice, *J. Appl. Comput. Mech.*, xx(x), 2024, 1–13. <https://doi.org/10.22055/jacm.2024.46584.4556>

Publisher's Note Shahid Chamran University of Ahvaz remains neutral with regard to jurisdictional claims in published maps and institutional affiliations.

